# Technical Memorandum

**To:** T.A. Cody Gonzalez, Prof. Sherif Hassaan

**From:** Kevin Naraki Kim Wong, Triet Ho, Josue Guerrero, Devrajsinh Mayurdhvajsinh Zala, Matthew Valencia, Noah Palanjan, Tristan Reyes, Vanessa Abigail Renderos, Yonghao Huo, Xuanqi Zang.

**Subject:** Lab 2 Drag of Simple Shapes and Calibration of Force Balance

**Due Date:** October 31, 2024

**Date of Experiment:** October 17, 2024

**Abstract:**

The objective of this experiment was to analyze the drag characteristics of simple shapes, including spheres, tripped spheres, and cylinders, using a wind tunnel. The goal of the experiment was to calibrate a force balance system and measure the drag forces exerted on these objects at various air speeds. Using acquired drag data, the Reynolds number and drag coefficients were calculated, enabling a comparison between experimental results and theoretical predictions.

Furthermore, the experiment outlined the importance of steady airflow over shapes and surface selection at different velocities. Calibration weights were used to ensure the accuracy of the force balance. The results demonstrated the expected relationship between shape geometry, surface condition, and drag behavior, contributing to an understanding of fluid resistance and flow characteristics.

**Introduction:**

Drag is a fundamental concept in fluid mechanics, playing a significant role in determining the forces on objects moving through a fluid. Defined as the resistive force due to fluid flow, understanding drag across different shapes is essential in fields like aerospace engineering, automotive design, and sports. The drag force, FD can be expressed as:

$$F_D = \frac{1}{2}\rho V^2 C_D A \qquad \text{(Equation 1)}$$

where $\rho$ the fluid density, $V$ is the velocity of the object relative to the fluid, $A$ is the reference area, and $C_D$ is the coefficient of drag characterizing shape-specific drag properties.

The study of drag helps engineers optimize designs by minimizing resistive forces, thereby enhancing performance, efficiency, and safety. In aircraft, for example, reducing drag is essential for fuel efficiency and stability during flight. Similarly, in vehicles, minimizing drag improves aerodynamics and reduces fuel consumption.

Measuring and analyzing drag for different shapes provides valuable insights into how geometric factors influence fluid resistance. Simple shapes such as spheres, cylinders, and streamlined bodies are commonly used as models to analyze drag behavior under controlled conditions. These fundamental shapes allow researchers to investigate flow separation, boundary layer behavior, and the formation of turbulent wakes.

A primary method for assessing drag involves using a wind tunnel to simulate fluid flow over a body and measuring the forces exerted on it. Wind tunnels provide a controlled environment where airflow velocity and object orientation can be precisely adjusted. A force balance is typically employed to measure drag forces accurately, allowing for the calculation of the drag coefficient - a dimensionless parameter that characterizes a shape's drag properties. Calibrating the force balance is essential for accurate data, requiring comparison of the balance readings with known reference values.

The relationship between drag and the Reynolds number is also an important aspect of drag analysis. The Reynolds number, a dimensionless value characterizing the flow regime around an object, influences whether fluid flow is smooth (laminar) or transitions into turbulence. The Reynolds number is defined as:

$$Re = \frac{\rho V L}{\mu} \qquad \text{(Equation 2)}$$

where $L$ is the characteristic length along the direction of the flow (such as the diameter of the sphere or cylinder) and $\mu$ is the dynamic viscosity of the fluid. The experiment explores the relationship between $Re$ and $C_D$, observing how different shapes respond to varying flow conditions. Calibration of the force balance was achieved by applying known weights and comparing measured forces to theoretical values.

An outline for the memorandum is structured as follows: The procedure section will outline the experimental setup and procedures used to collect data. The results section will present the experimental results including plots of forces using the ATI system and Drag Coefficient versus Reynolds number figures. The discussion section will include a discussion of the accuracy of data collected, discrepancies (if applicable) and limitations of the equipment. A question section will answer questions addressed in the lab manual and finally a summary section will summarize critical results and provide a clear understanding of the experiment.

**Procedure:**

1) Schematic of the experimental setup

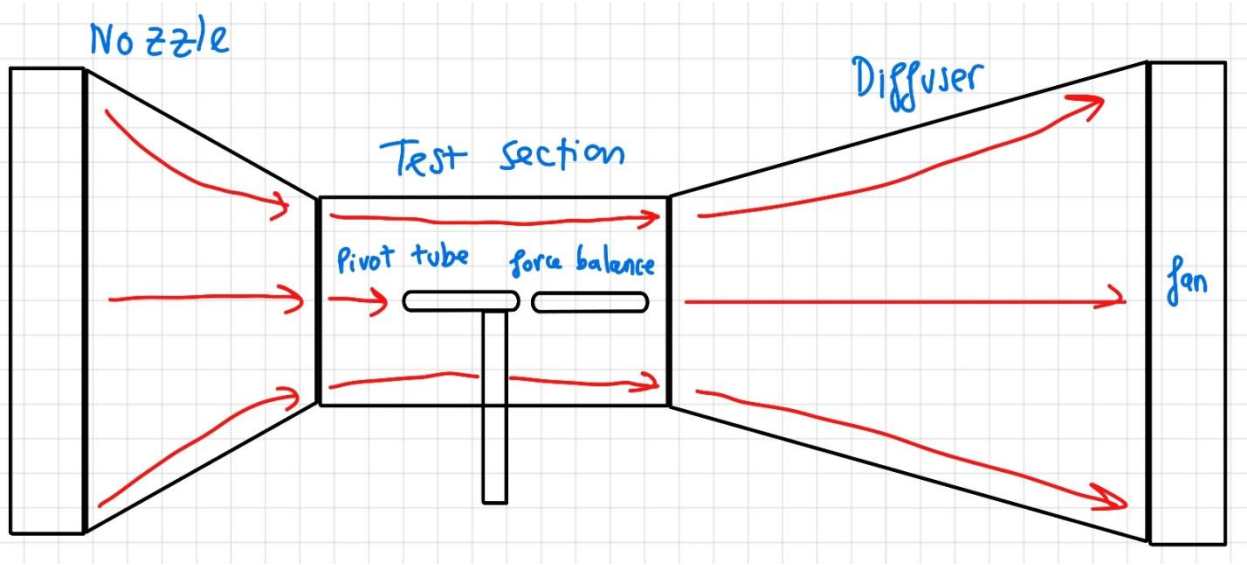


**Figure 1. Block Diagram of Experiment 2**

2) Experiment equipment

| Equipment | Description |
|---|---|
| Calipers | Used to accurately measure the diameter of the spheres and other test objects. |
| Leveler | Ensures that the test setup is leveled, allowing precise measurement of angles and alignment of the objects in the wind tunnel. |
| Digital balance | Measures the mass of the calibration weights for accurate force balance calibration. |
| LabView Software | Controls wind tunnel speed and collects data from sensors during the experiment. |
| Pitot-static tube | Measures the airflow velocity in the wind tunnel by sensing both dynamic and static pressure. |

| | |
|---|---|
| Sphere | A simple geometric object placed in the airflow to generate drag for testing. |
| Wire trip | A thin wire attached to the sphere, inducing turbulence to alter the drag characteristics. |
| Cylinder | Another geometric shape placed in the airflow to assess drag under varying flow conditions. |
| Streamlined Object | Designed to minimize drag, this object is used for comparison with other less aerodynamic shapes. |
| Setra Pressure Transducer | Captures differential pressure readings, providing key data on flow characteristics in the wind tunnel. |
| Force balancer | Measures the drag forces acting on various shapes, allowing for the calculation of drag coefficients across different velocities and conditions. |

3) Summary of lab procedures

Calibration of Force Transducer

a. Run a measurement and verify zero readings.

b. Configure a calibration weight (< 400 g), place it at one set position on the sting.

c. Run a measurement. Record and compare the measured forces and torque to the applied. Repeat with the weight at another location.

d. Repeat b and c with two more weights.

e. Repeat a, b, and c with three more angles of attack (two positive and one negative).

f. Plot your results of applied forces and torques vs. the measured forces and torques.

Drag on a Smooth Sphere

a. Measure the diameter of the sphere and mount it on the force balance.

b. Calibrate force transducer.

c. Install the Pitot-static tube 3 cm from the wall.

d. Set the velocity to 5, 15, 25, 35, 30, 20, 10, and 5 m/s and record the corresponding values for the axial force. Plot the $C_D$ vs. Reynolds Number.

e. For each velocity, record the dynamic pressure, axial force, use them to determine drag coefficient and Reynolds number.

f. Plot the drag coefficient as a function of Reynolds number.

Drag on Sphere with Wire Trip

a. Place the copper wire ring on the sphere with Scotch tape.

b. Repeat all the steps for the smooth-sphere measurements.

c. After recording, remove the sphere first, then remove the copper ring from the sphere.

Drag of a Streamlined Object

a. Mount the streamlined object on the force balance.

b. Following the procedure used in the smooth-sphere tests, determine the drag coefficient for the streamlined object as a function of Reynolds number.

Wall Effects Measurements

a. Record the length of the 4 cylinders and the width of the wind tunnel test section.

b. Mount 1 cylinder on the force balance. Set wind velocity to 35 m/s. Use the wall-mounted static taps to record the drag measurement Repeat with other cylinders.

**Results:**

(1).

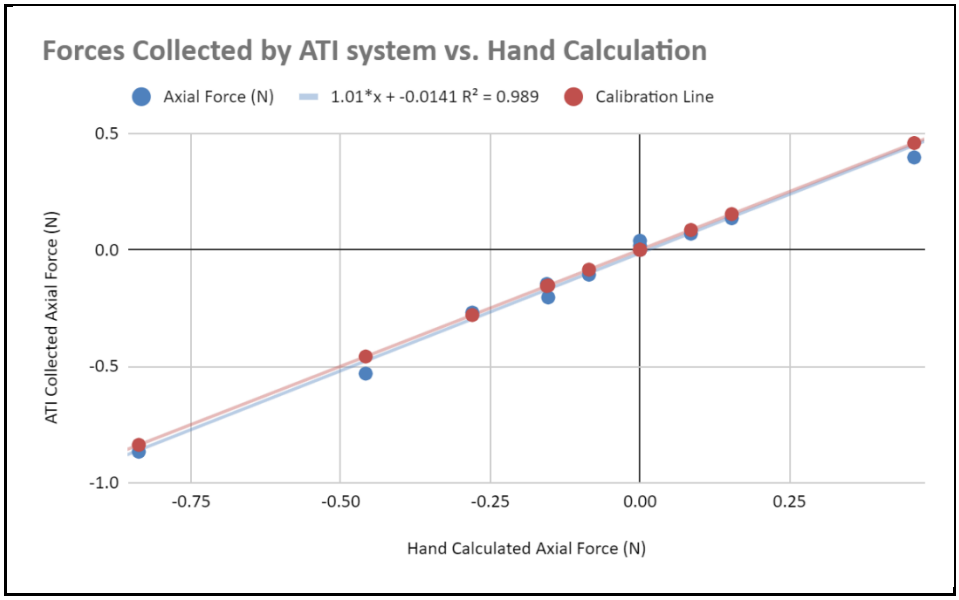


**Figure 2: The plot shows how the axial forces collected by the ATI system compare with axial forces obtained using hand calculation**

(2).

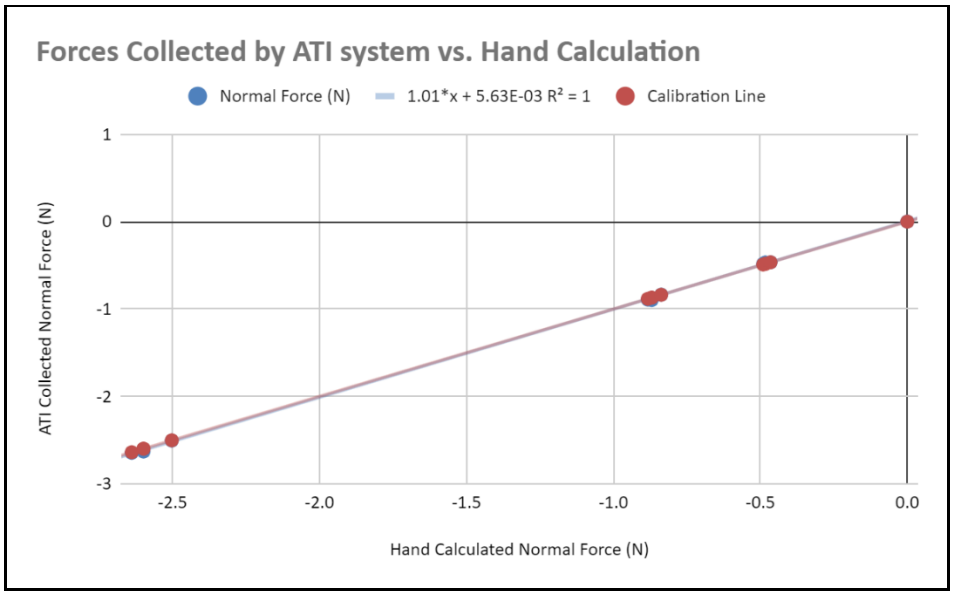


**Figure 3: The plot shows how the normal forces collected by the ATI system compare with normal forces obtained using hand calculation**

(3).

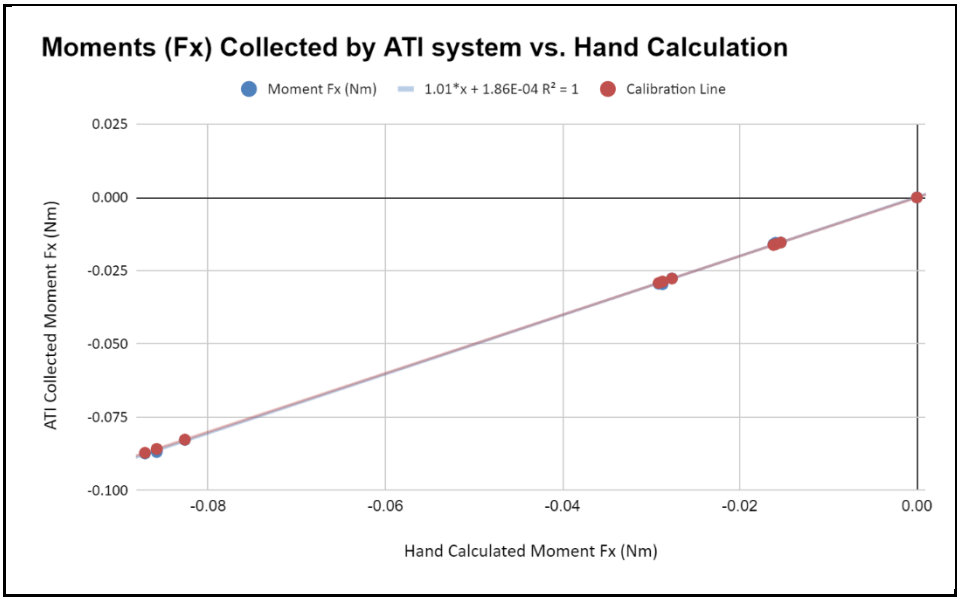


**Figure 4: The plot shows how moments (Fx) calculations collected by the ATI system compare with moments (Fx) obtained using hand calculation**

(4).

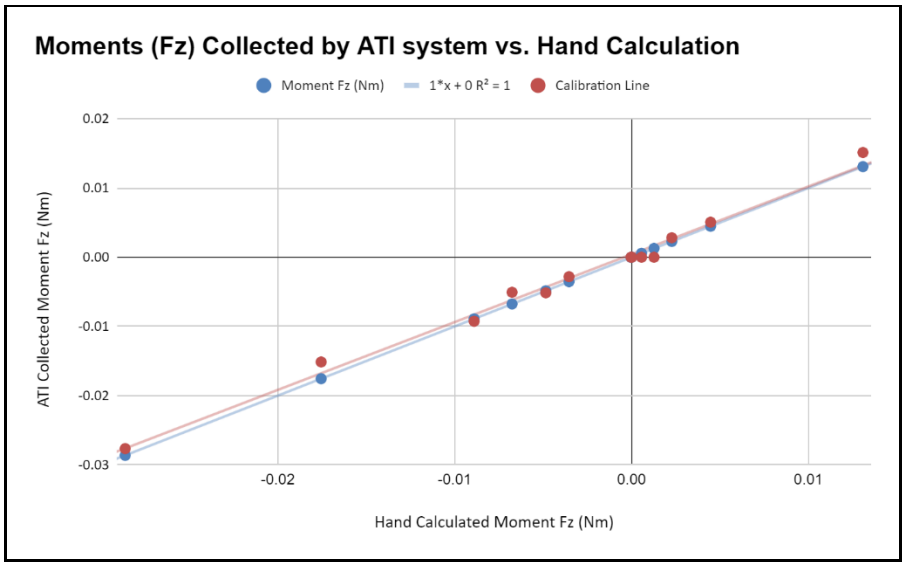


**Figure 5: The plot shows how moment (Fz) calculations collected by the ATI system compare with moments (Fz) obtained using hand calculation**

(5).

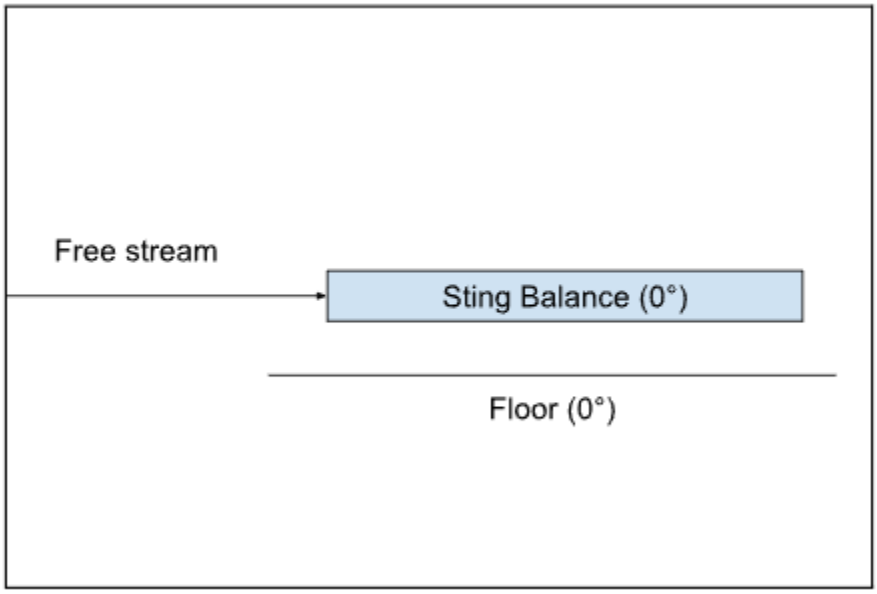


**Figure 6: Wind Tunnel Setup for Drag Force Measurement**

(6).

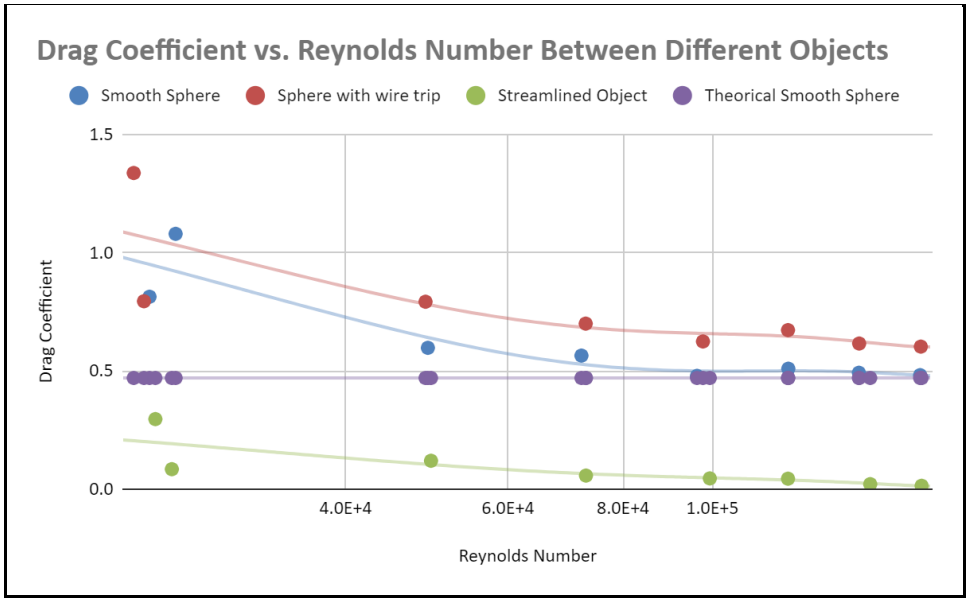


**Figure 7: Drag coefficient of smooth sphere, sphere with copper ring, streamlined object, and theoretical smooth sphere are plotted as a function of Reynolds number.**

(7).

**Table 1: Critical Reynolds number for different shapes**

| Shape | Critical Reynolds Number |
|---|---|
| Sphere | 2.5 x 104 |
| Tripped sphere | 9.8 x 104 |
| Streamlined body | 1.7 x 105 |

(8).

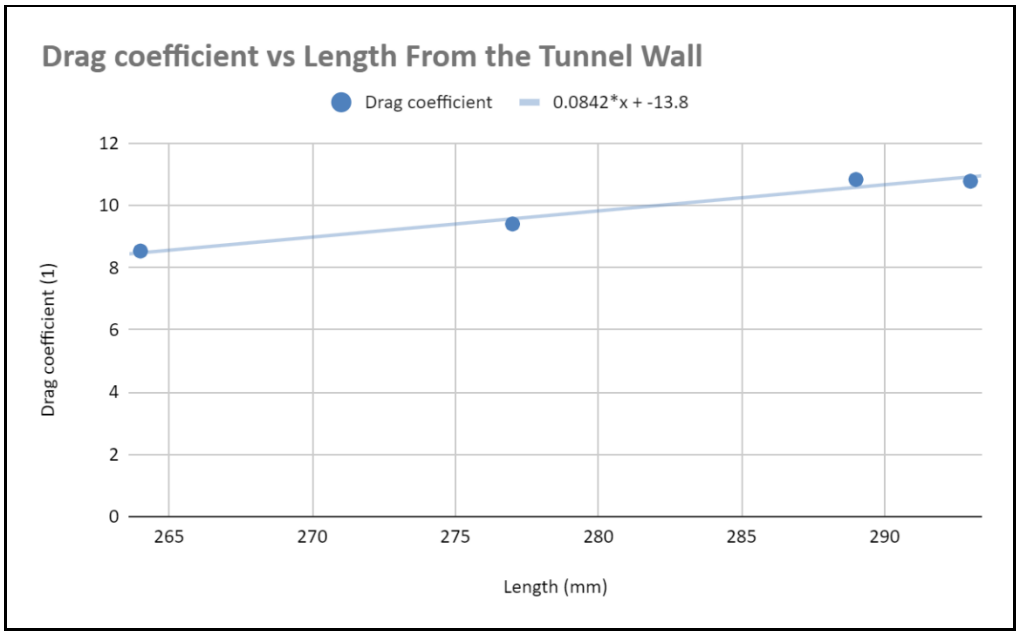


**Figure 8: Plot the drag coefficients of the cylinders as a function of the distance of the cylinder from the tunnel wall.**

**Discussion:**

Figure 2 shows the relationship between experimentally measured axial force and the hand-calculated axial force. The best-fit line equation is:

$$F = 1.01x - 0.0141 \quad \text{(Equation 3)}$$

This equation has an accuracy of $R^2 = 98.9\%$, indicating a very close fit to the data. In an ideal scenario, the equation would take the form:

$$F = 1x + 0 \quad \text{(Equation 4)}$$

Here, the slope of 1.01 is nearly identical to the ideal value of 1, and the y-intercept of -0.0141 is close to 0, showing minimal deviation from the expected value. Similarly, Figure 3 represents the relationship for normal force, with the best-fit equation given by:

$$F = 1.01x + 0.00563;\ R^2 = 1 \quad \text{(Equation 5)}$$

With an $R^2$ value of 1, the equation above shows the slope is approximately 1, and the y-intercept is approximately 0. Thus, the best-fit line of the data collected via the ATI system closely aligns with the ideal calibration line. The measured and expected values agree according to our results.

Figure 7 provides insight to the drag coefficient behavior for the different shapes we experimented. The drag coefficient is highest for a sphere with a wire strip, then decreases for a smooth sphere, and is lowest for a streamlined object. The results align with theoretical expectations - streamlined objects are designed to minimize drag by reducing boundary layer separation, contributing to the total drag. In contrast, the wire strip on the smooth sphere acts as an obstacle to airflow, increasing resistance. The experimental drag coefficient for a smooth sphere closely matches the theoretical value, especially at Reynolds number above $8\ x\ 10^4$.

**Questions:**

1. Which calibration values do you believe are more accurate (ATI output or hand calculations)? Why?

The ATI output calibration values are more accurate due to automated data acquisition, reducing human errors.

2. What should be the angle of the sting arm for the most accurate measurement of the drag coefficient? Why?

A 0-degree angle relative to the airflow ensures minimal interference, allowing accurate drag coefficient readings.

3. Contrast the drag coefficients for the four data sets (sphere, sphere with trip, streamlined object, and longest cylinder) at three Reynolds numbers (minimum, maximum, and a midpoint value) and explain reasons for any differences.

At high Reynolds numbers, drag coefficient decreases in the following order: cylinder, sphere with trip, sphere, and streamlined object (Figures 5 and 6).

For medium and low Reynolds numbers, there is no data for the longest cylinder; the drag coefficient decreases in the following order: sphere with trip, sphere, and streamlined object (Figure 5).

The data is consistent with aerodynamic principles because the streamlined object is designed to have a low drag coefficient, thus the smooth sphere should have a lower drag coefficient than the non-smooth sphere.

4. Qualitatively comment on the sources of uncertainty in the experimentally measured drag coefficients

Sources of uncertainty in the experimentally measured drag coefficients include instrumentation error from the force balance and sensors. Other factors include flow quality issues, such as turbulence within the wind tunnel, surface roughness affecting the boundary layer transition, noise in data acquisition systems, and variations in Reynolds number due to fluctuations in airflow speed or temperature. Additionally, during the procedure, it was observed that the sting arm lacked sufficient stiffness to adequately support the weight of the various objects, resulting in a downward tilt. Although the unbalanced sting arm was mitigated using a shim, it still introduced potential sources of error.

5. Can it be determined from the measured data what the value of the critical Reynolds number is for the smooth sphere or cylinder? How? What are the corresponding theoretical values (refer to your Fluid Mechanics text)?

The critical Reynolds number for a smooth sphere or cylinder can be determined from the measured data by identifying the point at which there is a sharp drop in the drag coefficient, indicating the transition from laminar to turbulent boundary layer flow.

For the smooth sphere in this experiment, the drag coefficient decreases significantly around $Re = 2.5x10^4$, suggesting a transition to turbulence in the boundary layer. For the tripped sphere with a wire trip to induce turbulence, the drag coefficient drops at a lower Reynolds number of around, $Re = 9.8x10^4$. The wire trip causes an earlier transition to turbulent flow, resulting in a lower critical Reynolds number than the smooth sphere. According to standard fluid mechanics textbooks, the theoretical, critical Reynolds number for a smooth sphere is approximately $Re = 2.5x10^5$, where the drag coefficient transitions from about 1.2 to 0.3 as the boundary layer becomes turbulent [2] [3]. For a cylinder, the critical Reynolds number is slightly lower, typically around $Re = 1x10^5$ [3].

In summary, the observed critical Reynolds number for the smooth sphere in this experiment is lower than the theoretical value. This discrepancy could be due to surface imperfections, minor experimental setup variations, or non-uniform airflow in the wind tunnel.

6. Compare the results of the cylinder drag measurements to standard, two-dimensional textbook values. What is the maximum distance from the wall at which the measured drag coefficient agrees with the standard textbook values? You can identify this distance as the maximum distance of an object from the wall for which the flow can be considered two-dimensional.

The data from Figure 7 shows that the drag coefficient increases as the distance from the wall increases. Ideally, as the cylinder moves farther from the wind tunnel wall, the drag coefficient should stabilize and approach the standard two-dimensional values, as wall interference effects diminish. However, in this experiment we observed an opposite trend, suggesting potential sources of flow interference or measurement errors. Another source could be non-uniform flow conditions due to blockages in the wind tunnel. In standard two-dimensional flow, the drag coefficient for a cylinder should be around 1.5. However, our experimental drag coefficient values never approached 1.5 at any measured distance from the wall, rather values near 8.5. The following linear relationship estimates the distance from the wall when $C_D$ = 1.5.

$$C_D = 0.0842x - 13.8 \qquad \text{(Equation 6)}$$

Solving for x yields a distance of 181.71mm, which is closer to the test section wall than any of our measured data points. This suggests an inconsistency, as purely two-dimensional effects would theoretically require placing the cylinder farther from the wall, contradicting the expected behavior in a wind tunnel. The experiment would require repositioning the cylinder close to the test section wall and minimizing any interferences for an improved value.

**Summary:**

This experiment evaluated the drag coefficients of various simple shapes, demonstrating the significant effects of geometry and surface conditions on drag. Key properties measured or calculated included drag force, drag coefficient, and Reynolds number.

To assess drag and measure forces, a wind tunnel was used in conjunction with a force balance, measuring the drag on each object. Different shapes for testing were mounted on a sting arm within the wind tunnel, and airflow was varied to simulate different Reynolds numbers. Data was collected at multiple speeds, allowing for analysis of the effects of surface roughness and object geometry.

The results aligned closely with theoretical predictions, higher drag for non-streamlined shapes and lower drag for streamlined objects. Experiment 2 emphasized the importance of precise calibration, surface conditions, and probe alignment for ensuring reliable data. A suggestion for future experimental topics should include a focus on reducing calibration errors and exploring advanced geometries to test for drag minimization.

**References:**

[1]. MAE 108 Laboratory Manual

[2]. Viscous Fluid Dynamics

[3.]. Beginners Guide to Aeronautics

**Signature box**

| | |
|---|---|
| Kevin Naraki Kim Wong |  |
| Triet Ho |  |
| Josue Guerrero |  |
| Devrajsinh Mayurdhvajsinh Zala |  |
| Matthew Valencia |  |
| Noah Palanjan |  |
| Tristan Reyes |  |
| Vanessa Abigail Renderos |  |

| | |
|---|---|
| Yonghao Huo |  |
| Xuanqi Zang |  |

**Appendices:**

## Appendix 1: Sample computations

This section will include sample computations that were done to reduce the data down to the final results.

Figure 2 calculations:

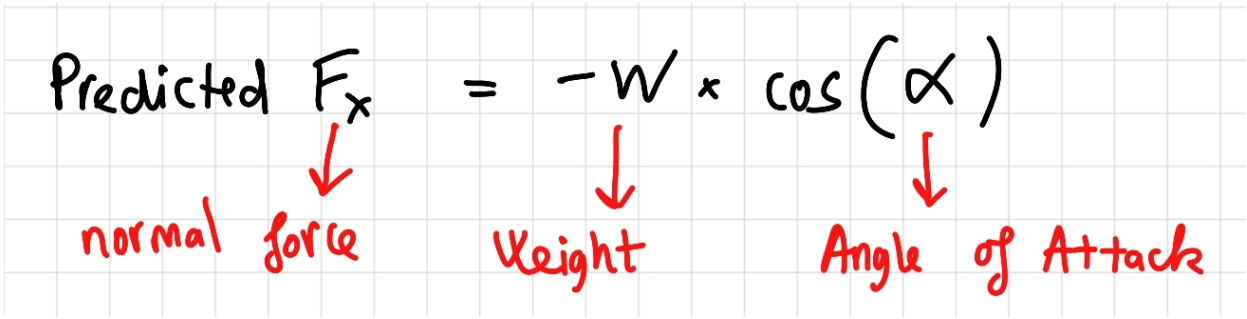


Figure 3 calculations:

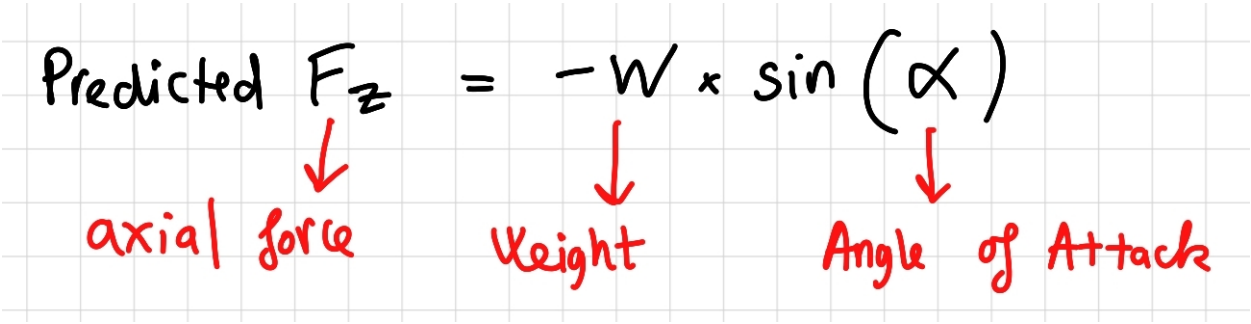


Figure 7 calculations:

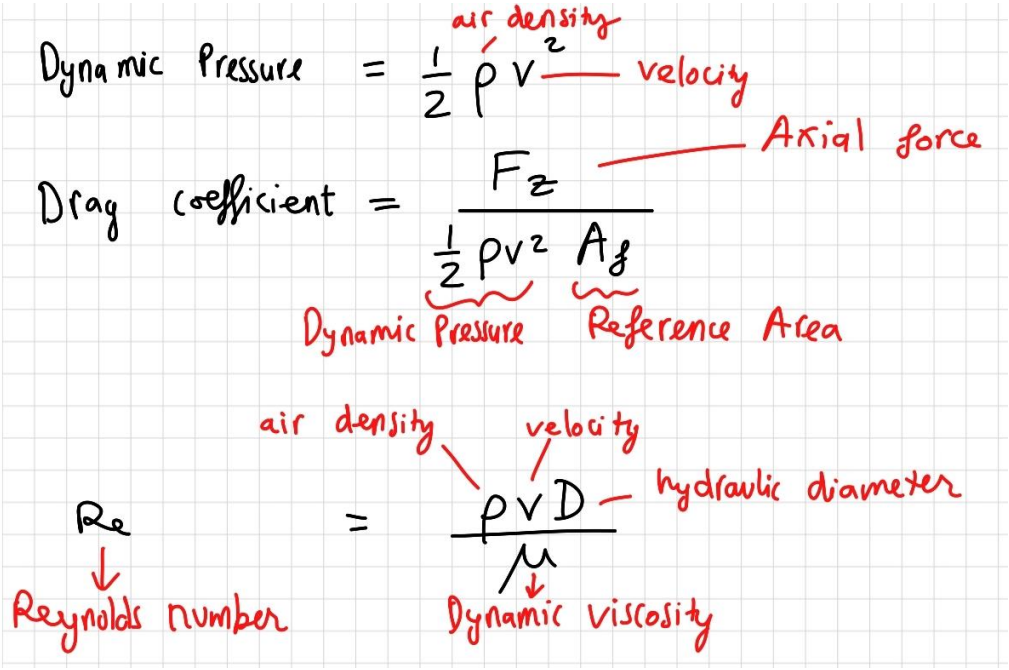

Figure 8 calculations:

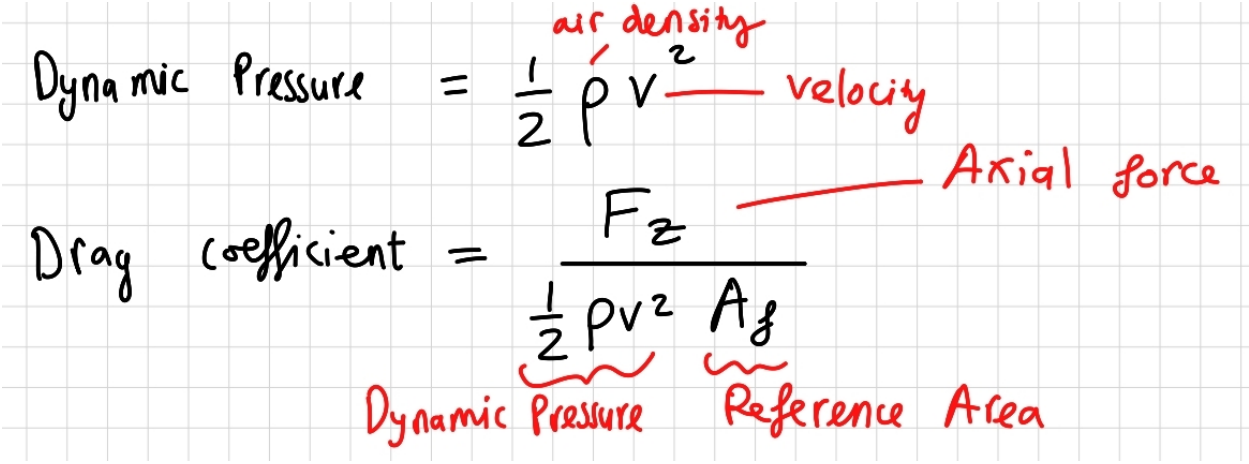

## Appendix 2: Experimental data

The following chart shows recorded data from the experiment.

**Table 2: Calibration of force transducer**

| Fx (N) | Fz (N) | Fx predicted (gram) | Fz predicted (gram) | angle of attack (degree) | Actual weight (gram) |
|---|---|---|---|---|---|
| 0.00104262 | -0.000787753 | 0 | 0 | 0 | 0 |
| -0.482592 | 0.000381866 | -50 | 0 | 0 | 50 |
| -0.891709 | 0.0385978 | -90 | 0 | 0 | 90 |
| -2.64598 | 0.0172322 | -269 | 0 | 0 | 269 |
| -0.467669 | 0.0690121 | -49.24038765 | 8.682408883 | -10 | 50 |
| -0.872784 | 0.13546 | -88.63269777 | 15.62833599 | -10 | 90 |
| -2.61509 | 0.396323 | -264.9132856 | 46.71135979 | -10 | 269 |
| -0.46948 | -0.106966 | -49.24038765 | -8.682408883 | 10 | 50 |
| -0.89667500 | -0.204446 | -88.63269777 | -15.62833599 | 10 | 90 |
| -2.6313 | -0.531359 | -264.9132856 | -46.71135979 | 10 | 269 |
| -0.464838 | -0.14669 | -47.41618276 | -15.86523282 | 18.5 | 50 |
| -0.835775 | -0.269405 | -85.34912897 | -28.55741908 | 18.5 | 90 |
| -2.50577 | -0.866826 | -255.0990633 | -85.35495257 | 18.5 | 269 |

**Table 3: Calibration of force transducer with calculated Moments**

| Moment Fx (Nm) | Hand Calculated Moment Fx (Nm) | Moment Fz (Nm) | Hand Calculated Moment Fz (Nm) | Distance (m) | Distance (inches) |
|---|---|---|---|---|---|
| 0.0000344273124 | 0 | -0.00002601160406 | 0 | 0.03302 | 1.3 |
| -0.01593518784 | -0.01619631 | 0.00001260921532 | 0 | | |
| -0.02944423118 | -0.029153358 | 0.001274499356 | 0 | | |
| -0.0873702596 | -0.0871361478 | 0.000569007244 | 0 | | |
| -0.01544243038 | -0.01595025166 | 0.002278779542 | 0.002812459716 | | |
| -0.02881932768 | -0.02871045298 | 0.0044728892 | 0.00506242749 | | |
| -0.0863502718 | -0.08581235392 | 0.01308658546 | 0.01513103327 | | |
| -0.0155022296 | -0.01595025166 | -0.00353201732 | -0.002812459716 | | |
| -0.0296082085 | -0.02871045298 | -0.00675080692 | -0.00506242749 | | |
| -0.086885526 | -0.08581235392 | -0.01754547418 | -0.01513103327 | | |
| -0.01534895076 | -0.0153593439 | -0.0048437038 | -0.00513916458 | | |
| -0.0275972905 | -0.02764681902 | -0.0088957531 | -0.009250496243 | | |
| -0.0827405254 | -0.08263327018 | -0.02862259452 | -0.02764870544 | | |

**Table 4: Drag on a Smooth Sphere**

| V (m/s) | Fx (N) | Fy (N) | Fz (N) | Tx (Nmm) | Ty (Nmm) | Tz (Nmm) |
|---|---|---|---|---|---|---|
| 5.088 | 0.024376 | 0.0122279 | -0.073302 | -0.301364 | -0.00168427 | 0.0117255 |
| 14.97 | 0.024493 | 0.00746277 | -0.349666 | 0.545808 | -1.93063 | -0.00446477 |
| 25.1 | -0.004369 | 0.0147277 | -0.8588 | -0.255225 | -6.65335 | 0.0126304 |
| 34.89 | -0.0327701 | 0.157806 | -1.55559 | -16.3689 | -11.5193 | 0.151521 |
| 29.94 | -0.045914 | 0.0670873 | -1.17407 | -5.71195 | -11.4172 | 0.177636 |
| 19.98 | 0.00869271 | -0.000164031 | -0.519126 | 1.56821 | -4.39328 | 0.259631 |
| 10.2 | 0.0274858 | 0.00733572 | -0.181021 | 0.434638 | -1.22025 | 0.0918399 |
| 5.431 | 0.0278967 | 0.00915635 | -0.101544 | 0.0796102 | -0.446316 | 0.0198741 |

**Table 5: Drag of Sphere with wire trip**

| V (m/s) | Fx (N) | Fy (N) | Fz (N) | Tx (Nmm) | Ty (Nmm) | Tz (Nmm) |
|---|---|---|---|---|---|---|
| 5.018 | 0.00692427 | -0.00632484 | -0.0529511 | 0.980132 | -0.836025 | 0.0761003 |
| 15.13 | -0.0349585 | -0.112415 | -0.420312 | 14.7707 | -10.3732 | 0.0784723 |
| 25.08 | -0.152217 | -0.316228 | -1.10865 | 41.2891 | -27.4171 | 0.203784 |
| 34.95 | -0.329422 | -0.614559 | -1.92936 | 79.3367 | -51.3204 | 0.704722 |
| 29.96 | -0.231489 | -0.471294 | -1.44859 | 60.9801 | -38.0025 | 0.612755 |
| 20.28 | -0.0656977 | -0.21403 | -0.673448 | 28.3003 | -16.222 | 0.538649 |
| 10.14 | 0.0201597 | -0.0418069 | -0.21403 | 6.47757 | -3.89182 | 0.206062 |
| 4.891 | 0.0364111 | 0.00402253 | -0.084314 | 0.867561 | -0.854461 | 0.213294 |

**Table 6: Drag of a streamlined object**

| V (m/s) | Fx (N) | Fy (N) | Fz (N) | Tx (Nmm) | Ty (Nmm) | Tz (Nmm) |
|---|---|---|---|---|---|---|
| 5.38 | -0.000620109 | 0.00208059 | -0.00531983 | 0.0190452 | 0.0982863 | 0.023082 |
| 15.14 | 0.0124709 | 0.00715793 | -0.0334037 | -0.907177 | 0.163733 | 0.0332446 |
| 25.08 | 0.0288571 | 0.0164679 | -0.0718699 | -2.75433 | 0.0633535 | -0.0259416 |
| 35.02 | 0.03020125 | 0.0375594 | -0.0447612 | -4.63123 | -0.127667 | 0.220773 |
| 30.8 | 0.0315454 | 0.0255982 | -0.0516459 | -3.68237 | 0.271823 | 0.160643 |
| 20.63 | 0.0131157 | 0.0142186 | -0.0496018 | -1.68503 | -0.0832181 | -0.0592732 |
| 10.28 | 0.00359808 | 0.0100398 | -0.0321639 | -0.309605 | -0.12779 | -0.112782 |
| 5.163 | -0.00112464 | 0.00864552 | -0.0196048 | 0.0278123 | -0.175125 | -0.101557 |

**Table 7: Wall effects measurements**

| V (m/s) | L(mm) | Fz_0 | Fx | Fy | Fz | Tx | Ty | Tz |
|---|---|---|---|---|---|---|---|---|
| 35 | 264 | 0.00563981 | 0.113754 | -0.045462 | -5.48693 | 32.1558 | -0.809234 | 2.36261 |
| 35.17 | 277 | 0.0323859 | 0.0046915 | -0.038118 | -6.07912 | 8.81306 | -3.76463 | 13.9456 |
| 35 | 289 | -0.0020402 | 0.11625 | 0.061346 | -6.97398 | 25.1438 | -4.14735 | 3.76995 |
| 35.06 | 293 | 0.00149196 | 0.192254 | -0.018776 | -6.95899 | 32.1427 | -4.48474 | 6.80544 |